Active control of a global thermocapillary instability

Junichiro Shiomi and Gustav Amberg
Department of Mechanics, Royal Institute of Technology (KTH), S-100 44 Stockholm, Sweden

(Received 9 January 2002; accepted 7 June 2002; published 2 August 2002)

Active control was applied to oscillatory thermocapillary flow in an open cylindrical container filled with Silicone oil. Thermocapillary convection was driven by imposing a radial temperature gradient on a flat free surface. This is an extension of the previous work by Shiomi *et al.* who applied proportional feedback control by locally heating the surface at a single position using the local temperature signal at a different position fed back through a simple algorithm. Although significant attenuation of the oscillation was detected, an uncertainty remained if global stabilization was achieved. In the present paper, two sensor/heater pairs were installed to achieve the global suppression of the oscillation. Successful global stabilization of the oscillation was achieved in a range of Marangoni number, with the best performance in the weakly nonlinear regime. Using a reliable temperature measurement method, quantitative analysis is carried out to quantify the performance of the control. The optimal values of gain and relative position of sensor/heater pairs were identified. © *2002 American Institute of Physics.* [DOI: 10.1063/1.1497375]

I. INTRODUCTION

In the floating zone method, a containerless method to produce single crystals, it is well know that the oscillatory state of the thermocapillary convection causes detrimental striations in the chemical composition of the finished crystal. Industrial need has motivated a number of experimental, theoretical, and numerical works to clarify the onset mechanism of the instability on various geometries commonly on half-zone models.[2–4] The present work attempts to suppress the oscillation by applying active control. While there is a strong motivation from the industrial application, this is also an attractive case for flow control in general, since it is a slow phenomenon with a limited number of modes active in the global instability, and stabilization of the flow can be done by measuring and modifying temperature which is usually easily accessible. Furthermore, the closed geometry makes feedback control possible.

One of the first to apply active feedback control through local modification of the temperature was Bau and coworkers, in a series of papers on control of thermal convection. For two-dimensional Rayleigh–Bénard convection, Tang and Bau[5] have theoretically demonstrated the possibility to delay the onset of the convection by almost one order of magnitude. This was followed by an experimental work of Howle[6] where the feedback control achieved significant suppression of two-dimensional convection in a slender box. The control method was also tested for three-dimensional convection by Tang and Bau,[7] where the obtained stabilization fell far short of the theoretical prediction done for two-dimensional convection.

There are only a few reported studies of active control of thermocapillary convection. An attempt to stabilize the thermocapillary wave instability in an experiment on a plane fluid layer has been made by Benz *et al.*[8] The temperature signal and the phase information sensed by thermocouples near the cold end of the layer was fed forward to control a laser which heated the downstream fluid surface along a line.

For an axisymmetric base state, Petrov *et al.*[9,10] attempted to stabilize the oscillation in a half-zone model, by applying a nonlinear control algorithm using local temperature measurements close to the free surface and heating a thermoelectric element placed at a location diametrically opposite the measurement. A successful control was observed at the sensor location for $\mathrm{Ma}\sim 17\,750$, however infrared visualization revealed the presence of standing waves with nodes at the feedback element and the sensor. This was resolved by adding a second sensor/heater pair which allows the control to damp out both waves propagating clockwise and counterclockwise and thus standing waves. The performance of the control was reported for a fixed $\mathrm{Ma}\sim 15\,000$, where the critical value was $\mathrm{Ma}\gtrsim 14\,000$.

The present study uses the annular configuration. In this geometry, a generic flow of a character similar to the one in the float zone method is studied.[11] As shown in Fig. 1, the system is an open cylindrical container filled with liquid to have a flat free upper surface. A heated pipe with a prescribed temperature is located on the axis of the container. The outer cylindrical wall is maintained at a lower temperature. Thermocapillary convection is thus driven by imposing a radial temperature gradient on the flat free surface.

Kamotani *et al.*[11] first demonstrated the thermocapillary oscillation in a cylindrical container of the annular type for high Pr. A three-dimensional oscillatory flow with a periodic surface temperature pattern was obtained. Comparing the data in normal gravity with the ones obtained in microgravity where the container size was varied, the upper limit of the container size below which Marangoni convection dominates over buoyancy convection was identified.[12,13] The major advantage of this geometry is that having the free surface perpendicular to gravity, it can be kept flat, thus better quantitative analysis can be achieved. The bottom temperature condition is adiabatic.

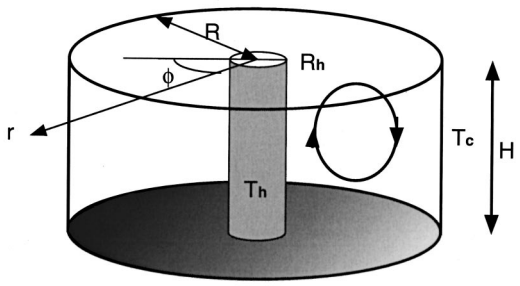

FIG. 1. Geometry.

This paper is a continuation of Shiomi *et al.*,[1] where we have attempted to apply the control method with a single sensor/heater pair. Although a significant attenuation was obtained at the sensor position, an uncertainty remained if the global stabilization was indeed achieved in all cases. More detailed measurements with multiple sensors in various azimuthal positions have suggested that evaluating the control scheme with single sensor signal could lead us to overestimation of the performance. As reported by Petrov *et al.*,[10] applying control with one sensor/heater pair could change the mode to a standing wave with nodes at the probe positions.

II. EXPERIMENT

The Marangoni number is defined as $\mathrm{Ma}=\gamma\Delta TR/\mu\alpha$, $\Delta T=T_h-T_c$, where γ, α, and μ are the surface tension coefficient, thermal diffusivity and dynamic viscosity, respectively. T_h and T_c are the temperatures of the hot and cold walls. The temperature is nondimensionalized as $\theta=(T-T_c)/\Delta T$ throughout the analysis.

The experimental apparatus and procedure are the same as in Shiomi *et al.*,[1] where more details are given. The experimental setup is shown in Fig. 2. A radial temperature gradient was imposed along the free surface by circulating warm water through the pipe heater and cold water through the copper cylinder. The aspect ratio Ar (ratio between the height of the fluid H and the radius of the cell R) was kept 1. The ratio of the diameter of the heated pipe R_h to R is Hr $=0.21$.

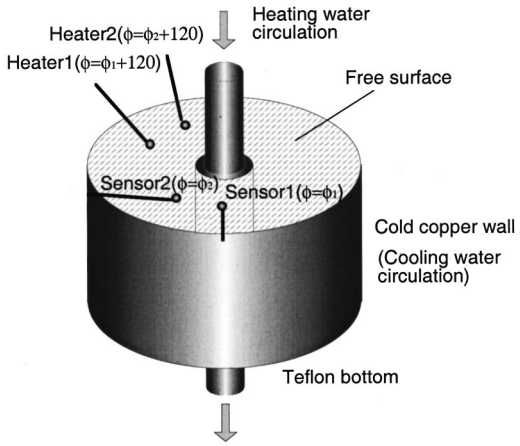

FIG. 2. Experimental setup.

The first step is to determine the azimuthal wave number. This was done by having two sensors in different azimuthal position and measuring the phase difference. For this particular geometry (Ar=1, Hr=0.21), the oscillation was found to have the azimuthal wave number of 3. Hence, placing the heater 120 degrees away in the azimuthal direction from the paired sensor, temperature oscillations at the positions would be in phase. A simple cancellation scheme is then realized by applying a voltage proportional to the inverted temperature fluctuation at sensor to a heater.

In order to control the two traveling waves with opposite direction of rotations, two sensor/heater pairs were installed as shown in Fig. 2. Sensor1 and Heater1 were positioned at $\phi=0°$ and $\phi=120°$, respectively, throughout the experiments. Sensor2 and Heater2 could be traversed along the azimuthal direction but their relative angle was kept at 120°. The radial positions of all the sensors and the heaters were at the midgap of the cell, $r=R_h+(R-R_h)/2$.

Having the temperature signals at two different azimuthal positions, clockwise and counterclockwise propagating waves can be identified. The amplitude of the oscillation based on the base frequency, $\hat{\theta}$ is the result of the superimposition of two waves with opposite direction of rotation as

$$\hat{\theta}(\phi,t)=A_1\sin n(\phi-\omega t+\eta_1)+A_2\sin n(\phi+\omega t+\eta_2), \tag{1}$$

where A_1 and A_2, are the amplitudes, and η_1 and η_2 are the phase of the clockwise and counterclockwise propagating waves, respectively. ω and n denote the frequency and the azimuthal wave number of the base frequency component. Utilizing the experimentally accessible values,

$$\hat{\theta}_1=\hat{\theta}(\phi_1,t),\quad \hat{\theta}_2=\hat{\theta}(\phi_2,t),\quad \frac{\partial\hat{\theta}_1}{\partial t},\quad \frac{\partial\hat{\theta}_2}{\partial t},\quad \omega,\quad n \tag{2}$$

we can solve for

$$A_1, A_2, \eta_1, \eta_2. \tag{3}$$

$\hat{\theta}$ was computed by applying a band-pass filter to pass the frequency component around the base frequency. ω corresponds to the peak of the power spectrum.

By reconstructing the two waves, we can clarify whether the wave structure is standing or traveling by comparing A_1 and A_2. As it was reported by Shiomi *et al.*,[1] traveling waves were observed in most cases. Occasionally, we did obtain $A_1\sim A_2$ when $(\epsilon\sim O(0))$, which suggests a standing wave. ϵ is the overcritical parameter defined as $\epsilon=(\mathrm{Ma}-\mathrm{Ma_{cr}})/\mathrm{Ma_{cr}}$. It seemed that standing waves were more likely to appear for smaller ϵ, however no conclusive tendency could be observed on the condition for a standing wave to appear.

The amplitude of the oscillation is $\sqrt{A_1^2+A_2^2}$ with A_1 and A_2 measured as described above. To confirm the accuracy of the temperature measuring technique and the reliability of the quantitative analysis, the bifurcation curve was drawn (Fig. 3). The uncontrolled part of all the measurements presented in this paper have contributed to this figure. Fitting a bifurcation curve to the data giving the points close to the

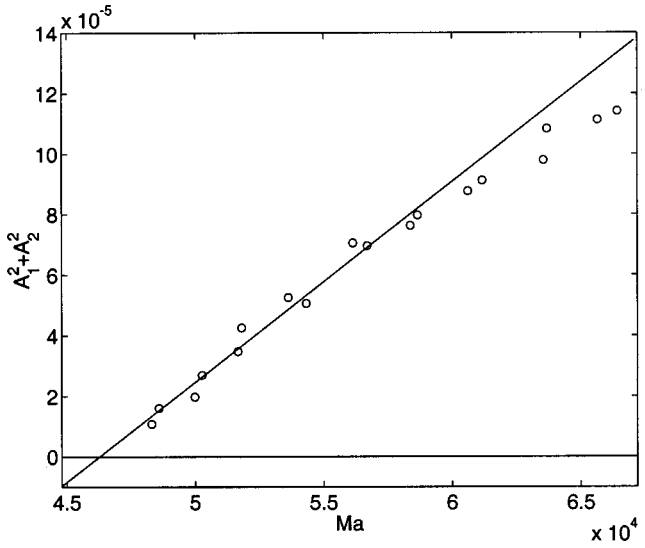

FIG. 3. Circles, the amplitude of the oscillation without control. Line, the square root curve fit to the data. Interpolating the line to $\sqrt{A_1^2+A_2^2}=0$, we obtained the critical Marangoni number $\mathrm{Ma}_{cr}=46\,270$.

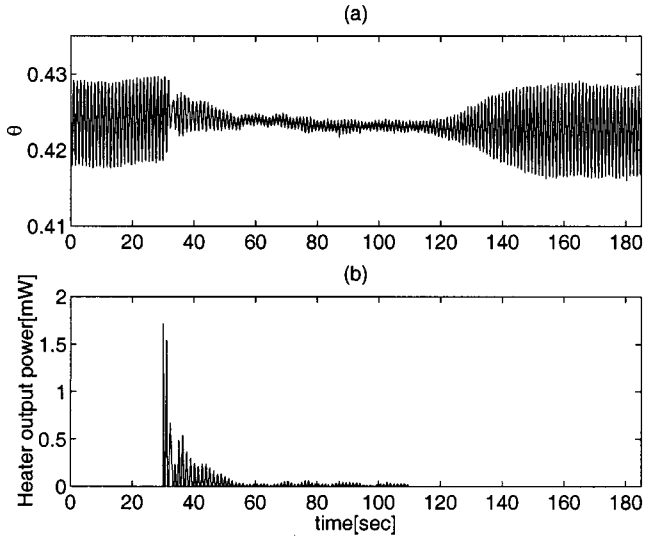

FIG. 5. (a) Time history of the temperature signal obtained from Sensor1. $\theta=(T-T_c)/\Delta T$, where T is the local temperature, T_c is the cold wall temperature, and ΔT is the imposed temperature difference. (b) Simultaneously measured heater output power: $\epsilon=0.08$, $d\phi=90°$.

bifurcation a large weight, a good agreement with supercritical Hopf bifurcation[14] was obtained in the weakly nonlinear regime. The plots fall beneath the bifurcation curve as the nonlinearity becomes stronger. By extrapolating the curve down to the criticality, the critical Marangoni number was found to be $\mathrm{Ma}_{cr}=46\,438$.

The gain of the control is set manually. For each Ma, the gain was varied to find its optimal value, i.e., the gain giving the smallest suppression ratio $\gamma(G_{\mathrm{opt}})$. γ is the ratio of $\sqrt{A_1^2+A_2^2}$ with control to the one without. Typical pictures of the gain dependency of the control performance is shown in Fig. 4. Here the gain is the ratio between the heater output voltage to the output voltage from the sensor system which is proportional to the local temperature. Starting from the smallest gain, the suppression ratio decreases as gain increases. As the gain exceeds the optimal value, the scheme loses the control and the system becomes chaotic.

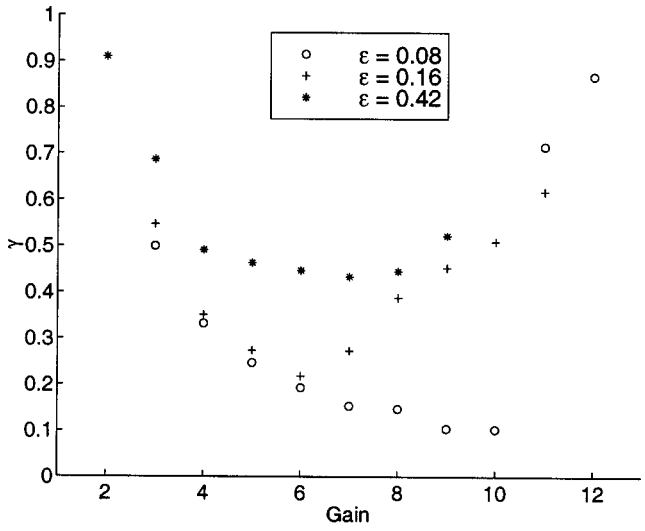

FIG. 4. The suppression ratio for various values of control gain. γ, ratio of the amplitudes with and without control: $\epsilon=(\mathrm{Ma}-\mathrm{Ma}_{cr})/\mathrm{Ma}_{cr}$.

III. RESULTS

A. Weakly nonlinear regime

The measurements were done for a range of ϵ. In Fig. 5 the result obtained for $\epsilon=0.08$ is shown. Another important parameter is $d\phi$, which is the angle between two sensor/heater pairs ($\phi 1-\phi 2$). Here the result from $d\phi=90°$ is presented since it turned out to give the best performance in a range of ϵ. The influence of $d\phi$ will be discussed further in a later section. When $d\phi=90°$, and the azimuthal wave number is 3, the phase difference of two signals is one-fourth of the period of the oscillation.

Figure 5(a) shows the time history of the temperature signal at Sensor1, where the control is successful to suppress the amplitude of the oscillation down to about 10% of the initial value. Turning on the control, the amplitude of the temperature oscillation was quickly suppressed to about 20% of the initial value. This is followed by a transient increase of the amplitude. Within a duration of about 20 seconds, the oscillation is gradually damped until the amplitude reached the minimum value. This state can be maintained indefinitely and is quantitatively repeatable. Note that the mean value of the oscillation has not changed before, during, and after applying the control. This indicates that the heat delivered to the fluid during the control is sufficiently small not to alter the base state appreciably. When the control was turned off, the oscillation slowly goes back to the initial state in about 30 seconds. A similar picture was obtained from the temperature signal at Sensor2 which indicates, this time, that global suppression is achieved.

The corresponding heater output power is shown in Fig. 5(b). The heater output of course follows the temperature signal. The initial overshoot reaches up to 1.5 mW, however,

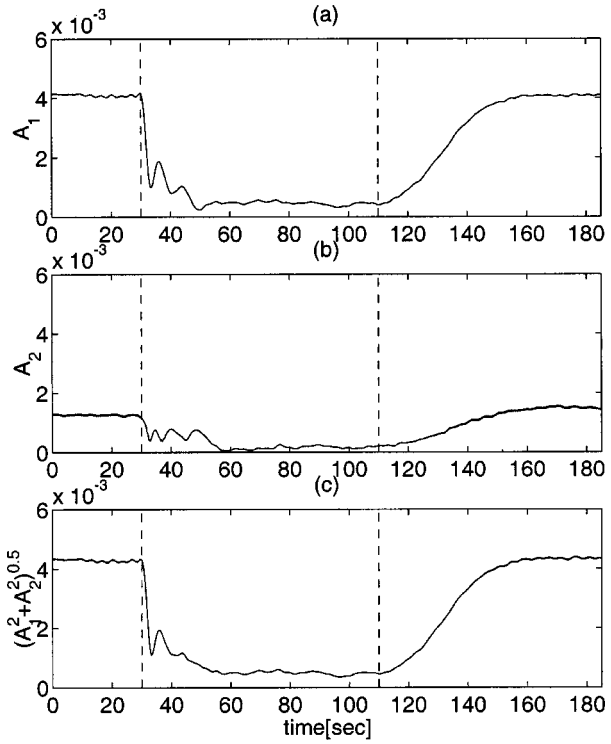

FIG. 6. Time history of the computed amplitudes of the waves propagating (a) clockwise, (b) counterclockwise, and (c) their superimposition. Dotted lines represent when the control was turned on/off: $\epsilon=0.08$, $d\phi=90°$.

once the periodic signals are stabilized, the state can be maintained with heater output no more than 50 μW.

Figure 6 describes the time history of the computed amplitudes of the waves propagating (a) clockwise, (b) counterclockwise, and (c) their superimposition for $\epsilon=0.08$. Since one of the two waves is dominant, the oscillation has a traveling structure when the control is not applied. Where the control was turned on/off are denoted with dotted lines. Major damping was achieved for both waves. Both amplitudes were suppressed to about 10% of their original values. As in the raw signal (Fig. 5), the amplitudes of two waves decay rather gradually over 20 seconds until it becomes almost constant around its minimum value. Turning off the control, both waves go back to the original states.

The power spectrum density for the signals in Fig. 5 ($\epsilon=0.08$) is shown in Fig. 7. The dashed line and the solid line represent spectra with control and without control, respectively. The spectra were calculated by taking more than 20 periods of basic oscillation into account. Here, the suppression of the oscillation can be confirmed by the significant decrease in energy around the base frequency. The first harmonic component has completely disappeared.

In some cases, we have observed that the direction of rotation changed before and after applying the control. In Fig. 8, we can observe that the oscillation which was dominated by clockwise rotating wave before applying the control is dominated by counterclockwise wave after turning off the control.

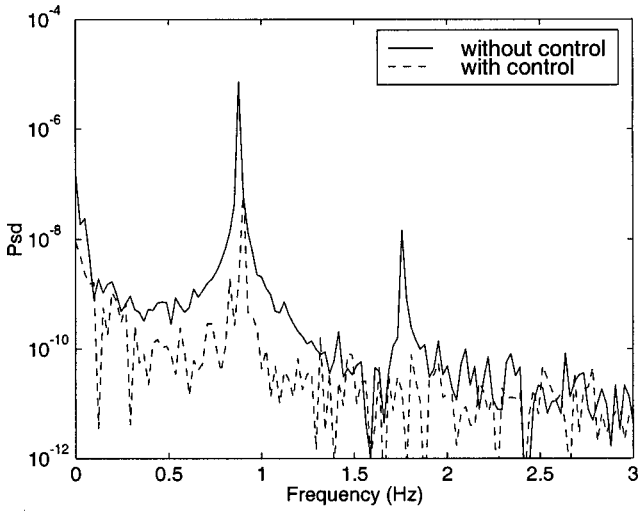

FIG. 7. The power spectrum density for the nondimensional temperature signal without control (solid line) and with control (dashed line): $\epsilon=0.08$, $d\phi=90°$.

B. Strongly nonlinear regime

The performance of the control shows different characteristics when the nonlinearity becomes stronger. The analysis of the amplitudes of two waves propagating clockwise and counterclockwise for $\epsilon=0.38$ is shown in Fig. 9. Compared with the weakly nonlinear case, an even stronger dominance of the counterclockwise propagating wave was observed, which implies that the wave structure is closer to a

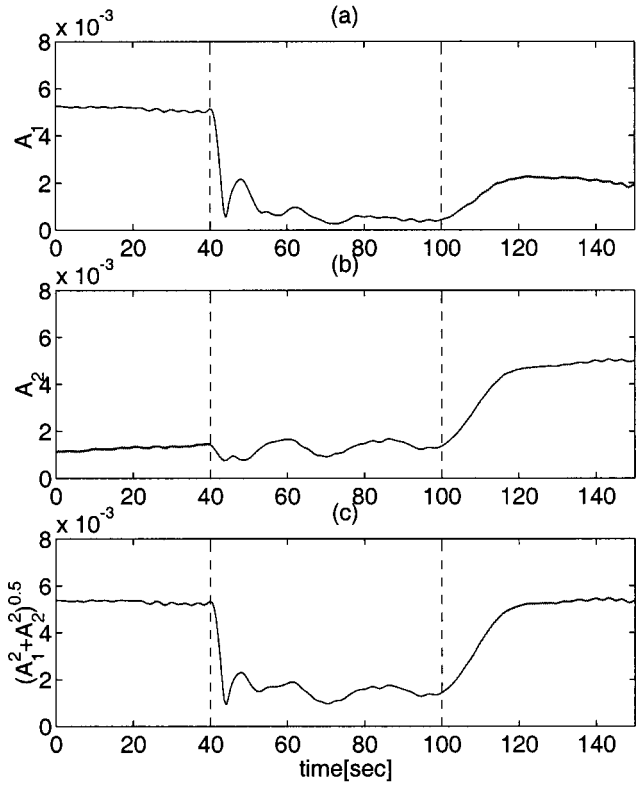

FIG. 8. Time history of the computed amplitudes of the waves propagating (a) clockwise, (b) counterclockwise, and (c) their superimposition. Solid lines represent when the control was turned on/off: $\epsilon=0.1$, $d\phi=60°$.

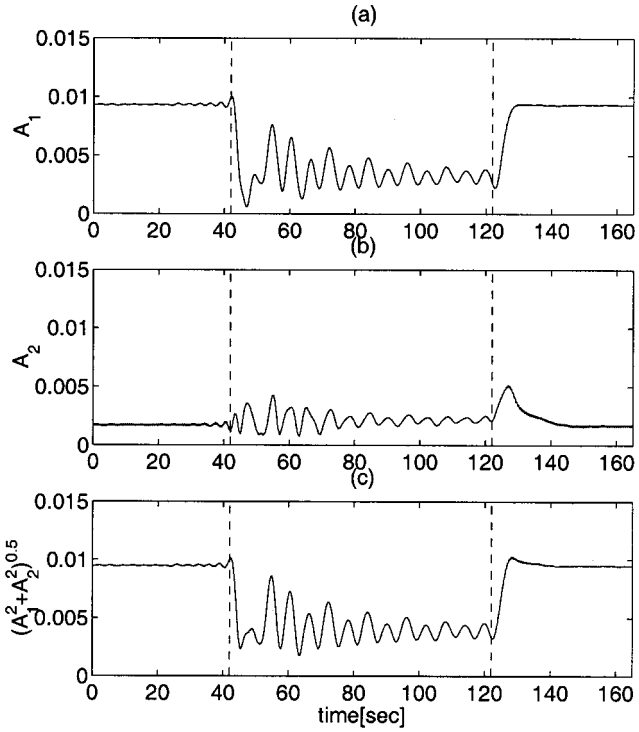

FIG. 9. Time history of the computed amplitudes of the waves propagating (a) clockwise, (b) counterclockwise, and (c) their superimposition. Solid lines represent when the control was turned on/off: $\epsilon=0.38$, $d\phi=90°$.

pure traveling wave. Even though significant attenuation of the oscillation is still obtained, the performance of the control falls short of the one seen for smaller ϵ. As in Fig. 9(c), turning on the control, the amplitude is immediately damped to 30% of the initial value. Then, as has been observed for small ϵ, the oscillation shows a transient increase. In this case this modulation is rather large and could not be completely damped within 80 seconds, though the amplitude of the envelope did decrease significantly. As discussed by Shiomi *et al.*,[1] the modulation may suggest the appearance of another mode being triggered by the control. The present positioning of sensors and heaters stabilizes mode 3, but could possibly destabilize the modes with other spatial structures. During the control, the amplitudes of the two waves become similar, which means that the oscillation has a standing structure. Removing the control, the oscillation quickly goes back to the initial state. The wave reversal as seen in the weakly nonlinear case was observed in this regime as well.

C. Performance of control

Overall performance of the control in a range of ϵ is presented in Fig. 10. Circles denote the values of $\gamma(G_{\mathrm{opt}})$ which is the suppression ratio γ at the optimal value of the gain G. The distance of two sensor/heater pairs in azimuthal direction is $d\phi=90°$. The best performance was obtained close to criticality. In the regime with weak nonlinearity, $\gamma(G_{\mathrm{opt}})$ increases rapidly with ϵ, except for $\epsilon\leqslant 0.12$ where $\gamma(G_{\mathrm{opt}})$ remains almost constant at its minimum. This minimum limit appears due to the random noise in the experiment. In this regime, the magnitude of the noise is comparable to that of the controlled signal.

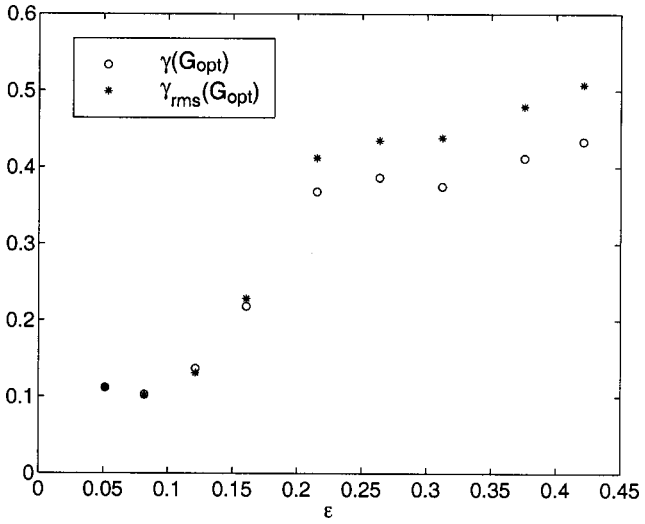

FIG. 10. Performance of the control over a range of ϵ. Circles, $\gamma(G_{\mathrm{opt}})$ computed from the amplitudes based on the base frequency. Stars, $\gamma_{\mathrm{rms}}(G_{\mathrm{opt}})$ computed from the amplitudes including harmonics: $d\phi=90°$.

When ϵ is above 0.22, the trend changes and $\gamma(G_{\mathrm{opt}})$ remains almost constant. Since the way we computed γ does not take harmonics into account, we have also shown the suppression ratio of the amplitudes with and without control computed by integrating the spectra of the signals over all the harmonic components. As the energy around the first harmonic frequency should make larger difference for stronger nonlinearity, stars start to deviate from the circles with increasing ϵ. However, the difference in magnitude is not so large that the performance of control should be doubted.

Petrov *et al.*[10] have achieved a successful control using a nonlinear control scheme for ϵ close to criticality ($\epsilon\leqslant 0.09$). However we have shown that in this range of ϵ, our linear control method is quite sufficient to stabilize the oscillation. Furthermore this simple and robust method has achieved significant attenuation of the oscillation for a range of $\epsilon\leqslant 0.42$. Here we need to keep in mind that these studies were done in different geometries. Comparing Fig. 7 with the spectrum shown by Petrov *et al.*[10] for similar ϵ, nonlinearity of the oscillation without control appears to be weaker for the half-zone model. This implies a possibility that this proportional control might work even better on the half-zone model.

D. Harmonic frequency

The energy growth in harmonic components was examined to seek for the correlation with the performance of control. Figure 11 shows the ratio of energy contained around the first harmonic frequency (E_{hf}) and the base frequency (E_{bf}) of the oscillations without (circles) and with control (stars). Without control, $E_{\mathrm{hf}}/E_{\mathrm{bf}}$ shows a simple increase proportional to ϵ. No distinct change in growth at $\epsilon=0.22$ was observed which might have caused the change in trend of control performance as we saw in Fig. 10. On the other hand, the data from controlled signals show a rapid increase

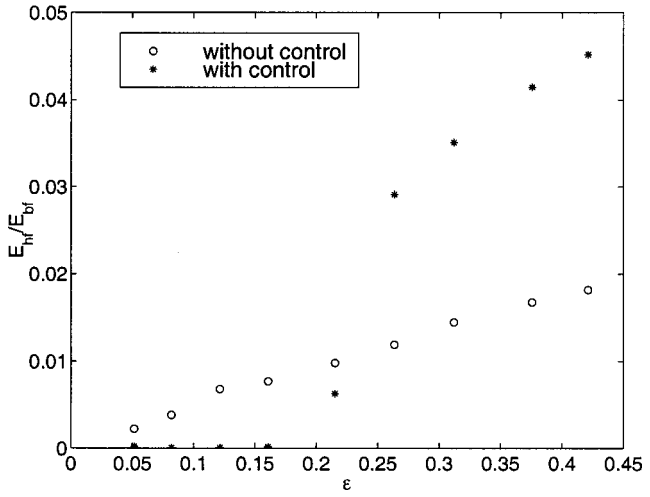

FIG. 11. The ratio of the energy around the first harmonic E_{hf} frequency to that around the base frequency E_{bf} for various values of ϵ.

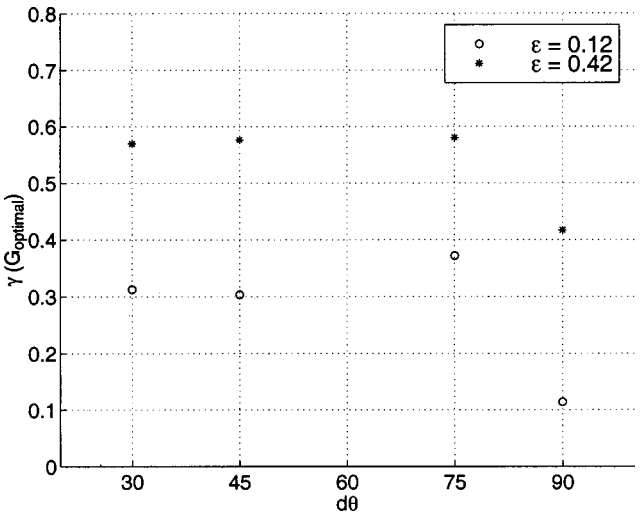

FIG. 13. Influence of $d\phi$ on performance of control.

of $(E_{hf})/(E_{bf})$ as ϵ crosses 0.22. In the strongly nonlinear regime, the energy around the first harmonic frequency E_{hf} is not suppressed, but it is rather amplified. This goes against the characteristic of this control method where any waves that are in phase at positions with distance of 120° should be suppressed to some extent. Although it is not clear yet what wave number the newly appearing mode has, it seems that it has a structure that its frequency component whose frequency is similar to the first harmonic of the fundamental frequency of mode 3 is amplified by the control with the present configuration of sensor/heaters.

E. Optimal gain

The optimal gain shows different characteristic in two regimes with weak and strong nonlinearity. As shown in Fig. 12, in the weakly nonlinear regime the optimal gain decreases with increasing ϵ. On the other hand, in the strongly nonlinear regime, the optimal gain remains constant. For the weakly nonlinear regime, scaling the optimal gain by multiplying it with the nondimensionalized amplitude of oscillation without control, the values fall within a range of 0.04–0.06. This way, for both weakly and strongly nonlinear regimes, the value of G_{opt} can be estimated from the resistance of the heater wire and the amplitude of the oscillation without control. This allows us to have the control method that is fully automatic.

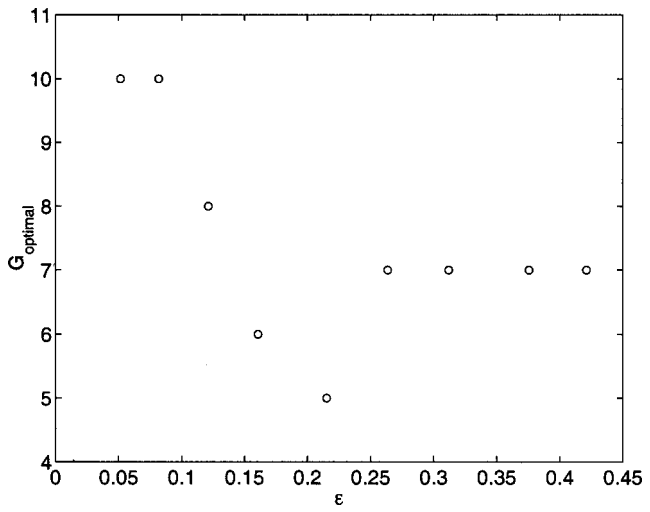

FIG. 12. Optimal gain for various values of ϵ.

F. Optimal $d\phi$

The influence of the relative position of two sensor/heater pairs on the performance of the control was analyzed. Figure 13 shows γ for different values of $d\phi$ in two regimes with weak and strong nonlinearity. Sufficient suppression was obtained for all $d\phi$ examined except for $d\phi=60°$. In this case, the control cannot capture the oscillation, since this positioning allows the wave to have nodes of the oscillation at both two sensor/heater pairs. No data are presented, since A_1 and A_2 cannot be computed when $d\phi=60°$. For a range of ϵ, the best control was achieved when $d\phi=90°$, and the rest performed to give similar values of $\gamma(G_{opt})$. At this stage, it is not clear if preferred spacing concerns the fundamental mode or the additional mode as well.

IV. CONCLUSION

Active control of oscillatory thermocapillary convection was carried out in an annular type geometry. Two sensor/heater pairs were installed to obtain a global stabilization of the oscillation. Significant attenuation of the oscillation was achieved in a range of ϵ, with the best performance when $\epsilon \geqslant 0.12$. In this regime, the oscillation is suppressed down to the level of the noise of the experiment. As the nonlinearity becomes stronger, $\gamma(G_{opt})$ increases until $\epsilon=0.22$ above which $\gamma(G_{opt})$ saturates and remains constant. The quantitative analysis was made possible by the reliable temperature measuring method which was confirmed by doing a bifurcation analysis on uncontrolled data. In the case of a strong nonlinear regime, the optimal gain remains constant, while in the weak nonlinear regime, multiplication of the optimal gain and the nondimensionalized temperature amplitude without control gives values in a small range (0.04–0.06). This en-

ables the control method to be fully automatic. The relative angle of two sensor/heater pairs were varied. Suppression was obtained in all the tested angles. The best relative position of two sensor/heater pairs was identified to be $d\phi = 90°$.

ACKNOWLEDGMENTS

We would like to thank Ulf Landén for his contribution on the experimental setup. This work was supported by the Swedish Research Council for Engineering Sciences (TFR).

[1] J. Shiomi, G. Amberg, and P. H. Alfredsson, "Active control of oscillatory thermocapillary convection," Phys. Rev. E **64**, 031205 (2001).
[2] F. Preisser, D. Schwabe, and A. Scharmann, "Steady and oscillatory thermocapillary convection in liquid columns with free cylindrical surface," J. Fluid Mech. **126**, 545 (1983).
[3] M. Levenstam and G. Amberg, "Hydrodynamical instabilities of thermocapillary flow in a half-zone," J. Fluid Mech. **297**, 357 (1995).
[4] M. Wanschura, V. M. Shvetsova, H. C. Kuhlmann, and H. J. Rath, "Convective instability mechanisms in thermocapillary liquid bridges," Phys. Fluids **7**, 912 (1995).
[5] J. Tang and H. H. Bau, "Feedback control stabilization of the no-motion state of a fluid confined in a horizontal, porous layer heated from below," J. Fluid Mech. **257**, 485 (1993).
[6] L. E. Howle, "Control of Rayleigh–Bénard convection in a small aspect ratio container," Int. J. Heat Mass Transf. **40**, 817 (1997).
[7] J. Tang and H. H. Bau, "Experiments on the stabilization of the no-motion state of a fluid layer heated from below and cooled from above," J. Fluid Mech. **363**, 153 (1998).
[8] S. Benz, P. Hinz, R. J. Riley, and G. P. Neitzel, "Instability of thermocapillary-buoyancy convection in shallow layers. Part 2. Suppression of hydrothermal waves," J. Fluid Mech. **359**, 165 (1998).
[9] V. Petrov, M. F. Schatz, K. A. Muehlner, S. J. VanHook, W. D. McCormick, J. B. Swift, and H. L. Swinney, "Nonlinear control of remote unstable states in a liquid bridge convection experiment," Phys. Rev. Lett. **77**, 3779 (1996).
[10] V. Petrov, A. Haaning, K. A. Muehlner, S. J. VanHook, and H. L. Swinney, "Model-independent nonlinear control algorithm with application to a liquid bridge experiment," Phys. Rev. E **58**, 427 (1998).
[11] Y. Kamotani, J. Lee, S. Ostrach, and A. Pline, "An experimental study of oscillatory thermocapillary convection in cylindrical containers," Phys. Fluids A **4**, 955 (1992).
[12] Y. Kamotani, J. Masud, and A. Pline, "Oscillatory convection due to combined buoyancy and thermocapillarity," J. Thermophys. Heat Transfer **10**, 102 (1996).
[13] Y. Kamotani, S. Ostrach, and J. Masud, "Microgravity experiments and analysis of oscillatory thermocapillary flows in cylindrical containers," J. Fluid Mech. **410**, 211 (2000).
[14] G. Iooss and D. D. Joseph, *Elementary Stability and Bifurcation Theory* (Springer-Verlag, Berlin, 1989).